Engineered Science
DOI: https://dx.doi.org/10.30919/es8d794

Pharmacokinetic, DFT Modeling, Molecular Docking, and Molecular Dynamics Simulation Approaches: Diptoindonesin A as a Potential Inhibitor of Sirtuin-1

Muhammad Ikhlas Abdjan,[1] Nanik Siti Aminah,[1, 2,*] Alfinda Novi Kristanti,[1, 2] Imam Siswanto,[1, 3] Mirza Ardella Saputra[4] and Yoshiaki Takaya[5]

Abstract

Sirtuin 1 (SIRT1) is a class III histone deacetylase that regulates several cellular processes. SIRT1 overexpression is found in many cancer cases and is a potential therapeutic target. Unlike resveratrol, several stilbenoid dimers have been identified as SIRT1 inhibitors. This work studied the interaction and dynamic behavior of stilbenoid dimers and SIRT1. Prediction of binding free energy (ΔG_{bind}) was calculated using the QM/MM-GBSA approach for each system, which resulted in 1NS-SIRT1: -21.44 kcal/mol, DS1-SIRT1: -25.94 kcal/mol, and DS2-SIRT1: -12.48 kcal/mol. These indicated that DS1 has a better chance as a SIRT1 inhibitor than DS2. The presence of glucose groups in DS1 potentially increased intermolecular interactions in the form of key residues and hydrogen bonds. Additionally, the quantum mechanical properties of DS1 and DS2 using the DFT/B3LYP/6-311++G(d,p) method were applied. The DS1 has three hydroxyls in the glucose group (3'-OH, 4'-OH, and 6'-OH) that could be reactive as nucleophiles and electrophiles. Furthermore, pharmacokinetic studies showcased the non-toxic properties of DS1. The analyses presented in this study could provide information on the quantum mechanical properties and inhibitory efficiency of stilbenoid dimers based on computational studies.

Keywords: Sirtuin-1; Diptoindonesin A; Quantum mechanics properties; QM/MM-GBSA approach; Computational studies.
Received: 05 July 2022; Revised: 26 November 2022; Accepted: 29 November 2022.
Article type: Research article.

1. Introduction

Sirtuins, or class III histone deacetylases, have seven enzymes (SIRT1-7) found in subcellular, such as cytoplasm, nucleus, and mitochondria.[1,2] It has been known that sirtuin enzyme activity was expressed in several cases of human cancers.[3–5] In particular, the enzyme sirtuin-1 (SIRT1) plays a role in cell proliferation and apoptosis.[6] Additionally, the SIRT1 enzyme also mediated the development of cancer cells through cell cycle pathways such as p53,[7] KU70,[8] RB1,[9] NFkB,[10] and FOXO.[2,9] Several previous studies have reported that the activity of the SIRT1 enzyme contributes to the growth of various types of tumors/cancer, such as prostate,[4,11] breast,[12,13] lung,[14] colon,[15] and ovarian.[16]

To date, studies on the activity of the SIRT1 enzyme are still controversial. SIRT1 has exhibited a pro-tumor and anti-tumor role in cancer regulation.[2,4] Therefore, this enzyme's mechanism of inhibition or activation is essential to study. Previous reports disclosed that SIRT1 inhibitors or activators could be obtained from either synthetic or natural product compounds.[17–20] Amongst these compounds, resveratrol, as part of stilbenoid natural products, was known to be the most effective SIRT1 activator.[21] However, the combination of resveratrol monomers in the form of dimers and tetramers also provided different activities as SIRT1 inhibitors.[19,20] In detail, the inhibitory activity of stilbenoid towards SIRT1 showed

[1] *Department of Chemistry, Faculty of Science and Technology, Universitas Airlangga, Surabaya 60115, Indonesia.*
[2] *Biotechnology of Tropical Medicinal Plants Research Group, Universitas Airlangga, Surabaya 60115, Indonesia.*
[3] *Bioinformatic Laboratory, UCoE Research Center for Bio-Molecule Engineering, Universitas Airlangga, Surabaya 60115, Indonesia.*
[4] *Nanotechnology Engineering, Faculty of Advanced Technology and Multidiscipline, Universitas Airlangga, Surabaya 60115, Indonesia.*
[5] *Department of Pharmaceutical Science, Faculty of Pharmacy, Meijo University, Nagoya 468-8502, Japan.*
**E-mail:* nanik-s-a@fst.unair.ac.id (N. S. Aminah)

promising results, namely from (-)-ampelopsin F (IC_{50} 24.4 μM) and (+)-hopeaphenol (IC_{50} 3.45 μM).[19] Meanwhile, the most effective synthesized compound to inhibit SIRT1 was EX-A5171 or 1NS (Fig. S1), which showed inhibitory activity IC_{50} of 4.00 nM.[17]

Diptoindonesin A (DS1) and ε-viniferin (DS2) (Fig. 1) are stilbenoid dimers isolated from the tree bark of *Shorea seminis* that is widely distributed in multiple Indonesian regions.[22] The stilbenoid dimers' structure consists of two resveratrol monomer units linked by a hydrofuran ring between regions A and B, as seen in ε-viniferin (DS2), one of the widely known stilbenoid dimers.[19,22] Unfortunately, ε-viniferin did not show any inhibitory effect on the SIRT1 enzyme at a concentration of 100 μM.[19] Meanwhile, Diptoindonesin A (DS1) is a new C-glucoside of ε-viniferin in which the glucose ring binds to the C-12b atom of the resveratrol region B monomer. The presence of this glucose group is expected to provide a better inhibitory activity than its core structure, ε-viniferin. This consideration is based on the presence of a glucose group that has a greater chance of interacting with the key residue at the SIRT1 enzyme binding site through hydrogen bond interactions. Thus, studying the interaction of stilbenoid dimers at the molecular level is essential. Previous studies have reported the interaction of stilbenoid tetramers with SIRT1 at the molecular level, but no reports for the dimers.[20] Therefore, molecular studies of the new C-glucoside of ε-viniferin are needed to understand its molecular interactions with SIRT1. Through these studies, we hope to understand the differences in molecular interactions between Diptoindonesin A and ε-viniferin against the SIRT1 enzyme.

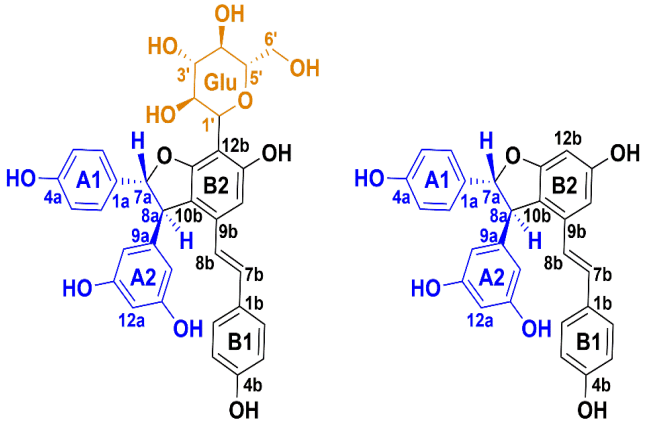

Fig. 1 The chemical structure of Diptoindonesin A (DS1) and ε-viniferin (DS2) labels in each region: blue for resveratrol region A, black for resveratrol region B, and orange for glucose.

Molecular studies are a reliable solution to understanding the interaction between stilbenoid derivatives and the SIRT1 enzyme.[20,23] It can be studied through a combination of molecular docking and molecular dynamics (MD) simulation, which has been widely used.[24] The evaluation of binding affinity is performed through the Quantum Mechanics/Molecular Mechanics-Generalized Born (QM/MM-GBSA) approach, which is known to have good reliability.[25,26] The binding affinity calculation requires much cost and time. However, it has accurate predictive results compared to conventional such as Molecular Mechanics (MM).[27] Meanwhile, quantum chemical modeling plays a crucial role in understanding the physicochemical properties of stilbenoid dimers. It also has been known that the density functional theory (DFT) method has advantages in studying the electronic structure of the molecule being modeled.[28–30]

The limitation of this research is that it only performs an analysis based on the prediction of the Diptoindonesin A activity against the SIRT1 enzyme through computational studies (*in silico*). Therefore, we recommend that further analysis should be carried out using *in vitro* and *in vivo* approaches in the future. The goal is to obtain a more comprehensive analysis in studying the interaction of Diptoindonesin A against the SIRT1 enzyme. The study conducted in this research is expected to provide insight at molecular level into the potential of Diptoindonesin A (a new C-glucoside of ε-viniferin) as an inhibitor of the SIRT1 enzyme.

2. Experimental section

2.1 Pharmacokinetic prediction

Diptoindonesin A (DS1) and ε-viniferin (DS2) were candidate compounds. The pkCSM server was used to calculate the pharmacokinetic properties such as absorption, distribution, metabolism, excretion, and toxicity (ADMET).[31] The calculation of ADMET properties used a 2D structure (SMILES format) for each candidate. The calculation process was used as an initial reference in seeing the candidate's biological activity as a criterion for a good drug.

2.2 Quantum chemical modeling

The quantum chemical calculations were performed by using the Gaussian 16W package. The geometry of the stilbenoid dimers was optimized using the DFT method with a Becke 3-parameter hybrid functional Lee-Yang-Parr (B3LYP).[32] The basis set of the molecular structure calculation of the stilbenoid dimers was 6-311++G(d,p). Several quantum chemical properties were then calculated, such as proton chemical shift, Fukui function, molecular electrostatic potential (MEP), and global reactivity. Calculating proton chemical shift was performed by the gauge independent

atomic orbital (GIAO) approach in the gas and solvation state.[33] The solvent model used was acetone with the integral equation formalism of the polarizable continuum model (IEFPCM). The results of the chemical shift modeling were calculated based on the corresponding TMS shielding at the GIAO/B3LYP/6-311+G(2d,p) level of theory as a reference. Parameters of correlation and accuracy between experimental and theoretical proton chemical shift were evaluated through statistical analysis, such as coefficient of determination (R^2 and R_0^2), absolute error/MAE (Eqn. 1), root mean square error/RMSE (Eqn. 2), and mean absolute percentage error/MAPE (Eqn. 3).

$$MAE = \frac{1}{n} \sum_{i=1}^{n} | \delta_i^{theo} - \delta_i^{exp} | \quad (1)$$

$$RMSE = \sqrt{\frac{1}{n} \sum_{i=1}^{n} (\delta_i^{theo} - \delta_i^{exp})^2} \quad (2)$$

$$MAPE = \frac{\sum_{i=1}^{n} \left| \frac{\delta_i^{theo} - \delta_i^{exp}}{\delta_i^{exp}} \right|}{n} \times 100 \quad (3)$$

Fukui function calculation aims to determine the most electrophilic (f_x^-) and nucleophilic (f_x^+) sites. These variables can be calculated using Eqns. 4 and 5. The variable Q shows the partial charge of each atom (x) of the modeled molecule. In summary, Q_x (M), Q_x (M-1), and Q_x (M+1) represent the electronic population of an atom (x), which has a neutral charge, cations, and anions. Meanwhile, Δf_x (Eqn. 6) shows the criteria for an atom (x) to be electrophilic when the value of $\Delta f_x > 0$ and nucleophilic $\Delta f_x < 0$.[34]

$$f_x^- = Q_x(M) - Q_x(M-1) \quad (4)$$

$$f_x^+ = Q_x(M+1) - Q_x(M) \quad (5)$$

$$\Delta f_x = f_x^+ - f_x^- \quad (6)$$

The charge distribution is visualized through molecular electrostatic potential (MEP) analysis. Electron density distribution in the form of HOMO-LUMO was studied through energy gap analysis (Eqn. 7). The distribution of electrons in the highest occupied molecular orbital (HOMO) and lowest unoccupied molecular orbital (LUMO) regions are the primary references in studying molecule reactivity. Several global reactivity parameters were calculated,[35] including electronegativity/x (Eqn. 8), chemical potential/μ (Eqn. 9), global hardness/η (Eqn. 10), global softness/s (Eqn. 11), and electrophilicity index/ω (Eqn. 12).

$$\Delta E_{gap} = E_{HOMO} - E_{LUMO} \quad (7)$$

$$x = -1/2(E_{LUMO} - E_{HOMO}) \quad (8)$$

$$\mu = -x \quad (9)$$

$$\eta = 1/2(E_{LUMO} - E_{HOMO}) \quad (10)$$

$$s = 1/2\eta \quad (11)$$

$$\omega = \mu^2/2\eta \quad (12)$$

2.3 Ligand and receptor preparation

The co-crystal structure of SIRT1 from the protein data bank (PDB ID: 4ZZI) was selected as the targeted protein. The native ligand EX-A5171 (PDB ID: 1NS) binds to the SIRT1 active site. This 1NS ligand is a SIRT1 inhibitor with good inhibitory activity.[17] The coordinate of 1NS ligand (control) and SIRT1 enzyme (receptor) from co-crystals was extracted using the Chimera 1.13 package, while the missing residues on receptors were rebuilt using Modeller 9.21 package. For the preparation of stilbenoid dimers (DS1 and DS2), the electrostatic potential (ESP) charges were calculated using DFT/B3LYP/6-311++G(d,p) method. Additionally, the addition of hydrogen atoms, AMBER FF14SB force field, and AM1-BCC aims to calculate missing parameters, such as bonded, non-bonded, and charge.

2.4 Molecular docking

The DOCK6 package performed all steps in molecular docking. The redocking stage aims to determine the binding site of the SIRT1 enzyme based on the 1NS coordinates. Several parameters were used in the redocking process, such as grid-spacing: 0.50 Å, center (X: 7.55, Y: 36.11, Z: -7.31), and dimensions (X: 28.86, Y: 27.32, Z: 23.51). The redocking stage is successful if the 1NS ligand superposition has an RMSD $\leq$ 2.0 Å.[36] Next, the stilbenoid dimers were docked on the SIRT1 enzyme based on the coordinates obtained in the redocking stage. The interaction energy in the molecular docking process was calculated using a grid score functional approach with the *anchor-and-grow* algorithm.[37]

2.5 Topology and system minimization

The simulation topology was prepared by tleap, which is available in the AMBER18 package. Topology preparation aims to produce a simulation system consisting of ligand, receptor, solvated receptor, complex, and solvated complex. The addition of the AMBER (FF14SB) force field was applied.[38] Preparation of solvated receptor and solvated complex used *solvatebox* TIP3PBOX (distance: 12 Å) with *source leaprc.water.tip3p*. The sodium ions (Na^+) were added randomly to neutralize the system, and the minimization process was carried out to minimize atomic contact and unfavorable steric hindrance in the system. The system was minimized in three stages: water molecules and sodium ions, ligand-receptor, and the whole system. The crucial parameters used in the minimization process were the steepest descent of 1500 steps and conjugate gradient of 500 steps. Lastly, the

calculation process used the *sander* tool available in the AMBER18 package.

2.6 Molecular dynamics simulation

The simulation process was performed through several stages, such as heating, density, equilibrium, and production, using *PMEMD.cuda* tool[39] contained in the AMBER18 package. The heating stage was carried out for 200 ps with a gradual temperature setting from 10 K to 310 K. The density stage was carried out for 300 ps at a temperature of 310 K. Next, the system was equilibrated for 1000 ps in settings with harmonic restraints of 30, 20, 10, and 5 kcal/mol/A^2. Finally, the whole system was produced under NPT ensemble conditions with a constant pressure of 1 atm and a temperature of 310 K for 100 ns. The production stage aims to create trajectories for further analysis and evaluation and is saved every 1000 ps per trajectory for evaluation purposes.

2.7 Trajectory analysis

Trajectory analysis was calculated using *cpptraj*[40] and *MMPBSA.py*[41] tools, which are also available in the AMBER18 package. The trajectory was calculated in the form of root-mean-square displacement (RMSD), atomic contacts, radius of gyration (RoG), water accessibility, and hydrogen bond (H-bond). Binding free energy (ΔG_{bind}) was calculated using the last 40 ns (160-200 ns) of the Quantum Mechanics/Molecular Mechanics-Generalized Born (QM/MM-GBSA) approach. Several critical parameters, such as the generalized Born solvation model: 2 and QM level theory: DFTB method, were used. The entropy change ($-T\Delta S$) was calculated based on the normal mode approximation (NMODE). Meanwhile, the calculation of free energy decomposition ($\Delta G_{bind}^{residue}$) utilized the Molecular Mechanics-Generalized Born (MM-GBSA) approach.

Mathematically, ΔG_{bind} can be calculated through Eqns. 13 and 14, which are the contribution of the enthalpy (ΔH) and entropy ($-T\Delta S$) changes.[42] More specifically, the contribution of free energy in the gas term (ΔG_{gas}) and solvation term (ΔG_{solv}) is responsible for the ΔH term. Meanwhile, the energy contribution to ΔG_{gas} consists of bonded energy (ΔE_{bonded}), van der Waals energy (ΔE_{vdW}), and electrostatic energy (ΔE_{ele}) (Eqn. 15). The ΔG_{bonded} shows the bond, angle, and torsion parameters, which have conformational energy equal to zero. Thus, the ΔG_{bonded} term can be neglected in calculating free energy. Moreover, the energy contribution to ΔG_{solv} consists of a generalized Born model (ΔG_{solv}^{ele}) and solvent-accessible surface area energy ($\Delta G_{solv}^{nonpolar}$) (Eqn. 16). In particular, the QM method produces a calculation parameter in the form of self-consistent energy (ΔG_{SCF}). In detail, the calculation of ΔG_{bind} can be calculated using the QM/MMGBSA approach (Eqn. 17).

$$\Delta G_{bind} = \Delta H - T\Delta S \quad (13)$$

$$\Delta G_{bind} = \Delta G_{gas} + \Delta G_{solv} - T\Delta S \quad (14)$$

$$\Delta G_{gas} = \Delta E_{bonded} + \Delta E_{vdW} + \Delta E_{ele} \quad (15)$$

$$\Delta G_{solv} = \Delta G_{solv}^{ele} + \Delta G_{solv}^{nonpolar} \quad (16)$$

$$\Delta G_{gas\ (QM/MM\text{-}GBSA)} = \Delta E_{vdW} + \Delta E_{ele} + \Delta G_{solv}^{ele} + \Delta G_{solv}^{nonpolar} + \Delta G_{SCF} - T\Delta S \quad (17)$$

3. Results and discussion

3.1 Pharmacokinetic properties of stilbenoid dimers

ADMET prediction of DS1 and DS2 compounds provided initial information on criteria for good drug candidates, as detailed in Table 1. DS1 and DS2 compounds were well absorbed into the human small intestine with an HIA value > 30%.[43] Both compounds showed the –BBB category with a log BB value < -1.00. It means these two compounds cannot penetrate the blood-brain barrier when they enter the body. Thus, they would not affect the work of the central nervous system.[44] Meanwhile, the effects of these two compounds on the body's metabolic cytochrome isoenzyme activity showed a positive result. In particular, compound DS1 did not interfere with the activities of these enzymes. Moreover, compounds DS1 and DS2 did not interfere with the work of renal OCT2, which contributes to renal excretion. Toxicity prediction

Table 1. Prediction of ADMET properties using pkCSM server.

Parameters	DS1	DS2
Absorption		
Intestinal Absorption-Human (% Absorbed)	75.90	90.84
Distribution		
BBB Permeability (log BB)	-1.44	-2.73
Metabolism		
CYP1A2 Inhibitor	No	No
CYP2C19 Inhibitor	No	Yes
CYP2C9 Inhibitor	No	Yes
CYP2D6 Inhibitor	No	No
CYP3A4 Inhibitor	No	No
Excretion		
Renal OCT2 Substrate	No	No
Toxicity		
AMES Toxicity	No	No
Hepatotoxicity	No	No
Skin Sensitisation	No	No

Intestinal Absorption-Human (+): HIA > 30% and Intestinal Absorption-Human (-): HIA < 30%. BBB Permeability (+): log BB > 0.30 and BBB Permeability (-): log BB < -1.00.

indicated that both compounds were non-toxic with the criteria of non-AMES toxicity, non-hepatotoxicity, and non-skin sensation. These are essential parameters in determining a particular compound as a promising drug candidate. Overall, the prediction of ADMET properties gave good results for DS1 and DS2 compounds.

3.2 Proton chemical shift

Chemical shift (proton) modeling was performed on gas and solution phases (acetone-IEFPCM) using the GIAO/B3LYP/6-311+G(2d,p) basis set as a reference approach. Using IEFPCM parameters on the solvent aims to stimulate the effect of the solvent. Determination of proton chemical shift (^{1}H-NMR) using the DFT method is considered more sensitive than carbon chemical shift (^{13}C-NMR) and has been widely applied by previous studies.[45–48] Proton chemical shift analysis offers a decisive fingerprint criterion for determining the dominant molecular structure in a solution.[48] Therefore, performing a proton chemical shift analysis using the DFT method.

Our previous work experimentally obtained proton chemical shifts of DS1 and DS2 compounds.[22] The calculation of the proton chemical shift of each compound showed a good correlation with the experimental results (Fig. 2). In detail, the proton chemical shifts of DS1 and DS2 are listed in Tables S1 and S2. Correlation results through linear regression analysis showed the value of R^2 and $R_0^2 \geq 90\%$ (Table 2), with the linear equations for each compound found to be y = 0.8817x + 0.7945 (in gas) and y = 0.9011x + 0.8112 (in acetone) for DS1 and y = 1.1594x - 1.1655 (in gas) and y = 1.1669x - 1.0558 (in acetone) for DS2. Meanwhile, the accuracy analysis between experimental and theoretical is presented by the MAE, RMSE, and MAPE parameters, as detailed in Table 2. Commonly, the smaller the parameter value, the better the accuracy results,[49] and particularly for the MAPE parameter, our results showed that each model has a MAPE ≤ 10%. It indicated that the accuracy of each model has excellent criteria and deserves further analysis. Overall, the statistical evaluation revealed promising results between experimental and theoretical.

3.3 Electronic structure properties

The optimized structure study aims to understand several electronic structure properties of stilbenoid dimers, including Fukui function, molecular electrostatic potential (MEP), and global reactivity. Fukui function is used to analyze the reactivity of each atom[34] and to determine each atom's nucleophilic and electrophilic properties in a modeled compound.[50] In this case, we describe the Fukui function of hydroxy groups in resveratrol monomer and glucose and esters in furan rings and glucose (Tables S3 and S4). This consideration is the possibility of hydrogen bond formation in the form of donors and acceptors of these atoms. The results disclosed several atoms in DS1 with high nucleophilicity ($\Delta f_x < 0$), such as 6'-OH, 3'-OH, and 13b-OH. Meanwhile, several atoms in DS1 served as the most electrophilic with $\Delta f_x > 0$, including 4'-OH, 3'-OH, and 4'-OH. On the other hand, DS2 only showed a 7a-O-11b atom as an electrophile. Interestingly, a glucose group in DS1 increased the number of atoms that have the potential to experience interactions compared to DS2. This parameter explained the reactivity difference between the two compounds. This was also supported by the visualization of MEP, which provided a representation of the charge distribution on the surface of the molecular structure (Fig. 3). The MEP analysis provided an overview of the most negative area (red > orange > yellow), the most positive area (blue > cyan), and a neutral area or zero charges, as shown in green. In general, the hydroxyl group (-OH) served as a nucleophile in both structures of these compounds.

Table 2. Statistical analysis: Accuration and correlation of proton chemical shift between experimental and theoretical for stilbenoid dimers.

Parameters	Gas	Acetone
DS1		
MAE	0.31	0.32
RMSE	0.39	0.40
MAPE	6.68	7.00
R^2	0.92	0.94
R_0^2	0.90	0.92
DS2		
MAE	0.21	0.16
RMSE	0.25	0.19
MAPE	3.47	2.53
R^2	0.93	0.96
R_0^2	0.91	0.94

Energy analysis at the orbital level provides information in viewing the molecule's electrochemical behavior,[51] HOMO (E_{HOMO}), LUMO (E_{LUMO}), and gap (ΔE_{gap}) energies were estimated by using DFT/B3LYP/6-311++G(d,p) in the gas state. HOMO orbitals act as electron donors and LUMO orbitals act as electron acceptors.[50,51] The HOMO-LUMO energy parameter was important in understanding the molecule reactivity. Additionally, these parameters became the primary reference in determining global reactivity, which is listed in Table 3. The results showed that the ΔE_{gap} difference between DS1 and DS2 was insignificant (~0.52 eV). It was observed from the lack of observable changes in each

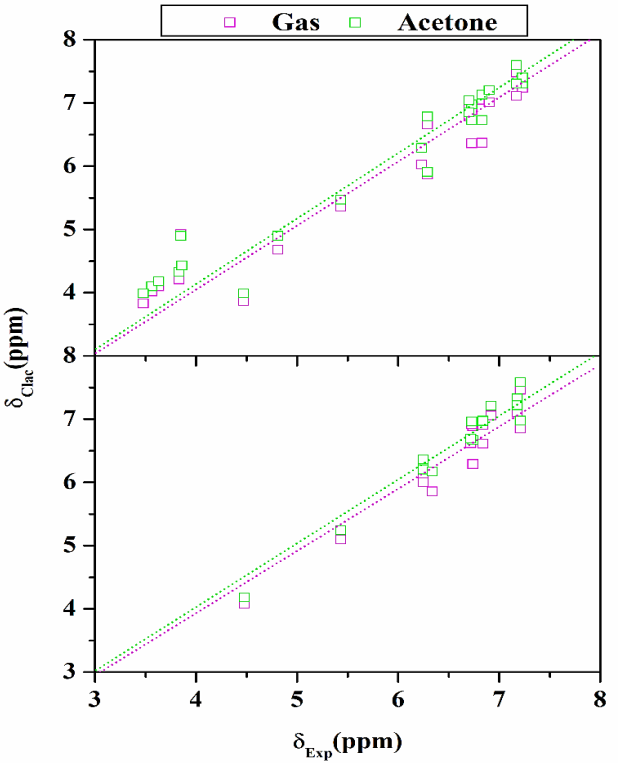

Fig. 2 Proton chemical shift between experimental (δ_{Exp}) and theoretical (δ_{Calc}). DS1 (top) and DS2 (bottom) compounds. The ^{1}H-NMR was calculated using the B3LYP/6-311+G(2d,p) level of theory as a reference.

molecule's HOMO and LUMO orbitals, which were located in the resveratrol region B structure. Meanwhile, the HOMO and LUMO orbitals in the resveratrol region A and the glucose were not visible (Fig. 4). From these, we can conclude that ΔE_{gap} was not affected by the presence of glucose on the DS1 molecule.

Table 3. Calculation of global reactivity was calculated using DFT/B3LYP-6-311++G(d,p) method in the gas state.

Molecular Properties	DS1 (eV)	DS2 (eV)
E_{HOMO}	-5.55	-5.60
E_{LUMO}	-1.67	-1.68
Electronegativity (x)	3.61	3.64
Chemical potential (μ)	-3.61	-3.64
Global hardness (η)	1.94	1.95
Global softness (s)	0.97	0.97
Electrophilicity index (ω)	3.36	3.38

3.4 Molecular docking analysis

Molecular docking analysis aims to determine the initial orientation of the ligand to the active site of a targeted protein.[36,37] The redocking process provides a clear picture of the active site coordinates based on the radius of the native ligand location (Fig. 5A). The obtained conformations are based on the selection of cluster spheres from a radius (10 Å) of 1NS ligand pockets. The redocking results showed an excellent superposition of 1NS with an RMSD value of 1.40 Å, which was supported by the previous report.[23] Furthermore, the docking process of DS1 and DS2 to the targeted protein occupied the SIRT1 binding site well. The scoring process used a grid score functional consisting of E_{vdW} + E_{ele} as the main contribution of the grid-score value (kcal/mol) in the gas term (Fig. 5B). It indicated that DS1 has a better grid score than DS2 and 1NS as a control. In addition, some amino acid residues were responsible for the interaction process with each

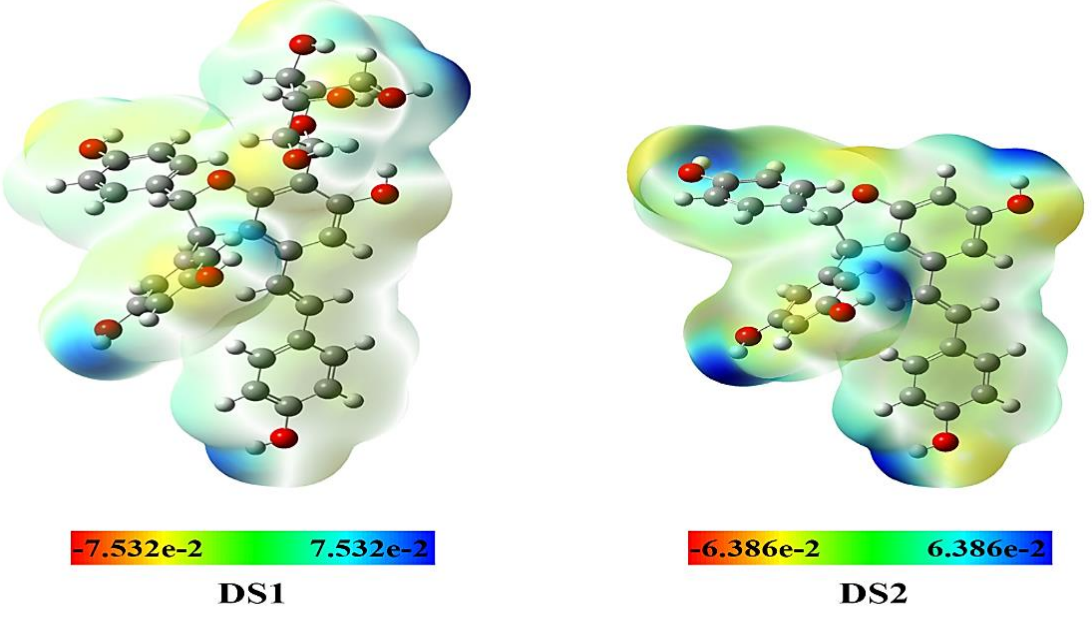

Fig. 3 Molecular electrostatic potential was calculated using DFT/B3LYP/6-311++G(d,p) method with isoval: 0.004. The red color represents negative charges, while the blue represents positive charges.

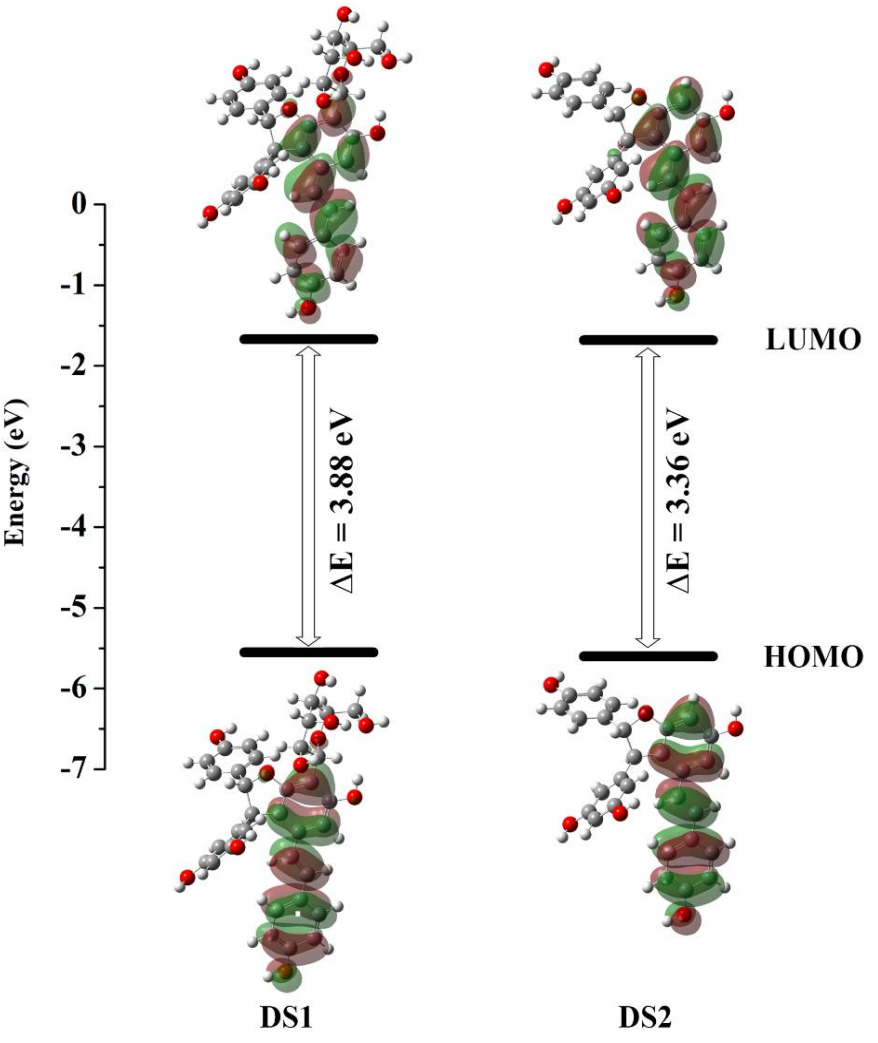

Fig. 4 HOMO and LUMO images of stilbenoid dimers. The ΔEgap (EHOMO-ELUMO) was calculated using DFT/B3LYP/6-311++G(d,p) method.

ligand, such as 1NS-SIRT1: ten residues (Fig. 5C), DS1-SIRT1: nine residues (Fig. 5D), and DS2-SIRT1: ten residues (Fig. 5E). However, it was essential to evaluate these results further using MD simulation to see the stability, per-residue energy decomposition, and binding affinity of each system. As discussed in the following section, the obtained coordinates from the docking process were used for further analysis purposes using MD simulation.

3.5 System stability

Integrating the obtained coordinates from molecular docking into the MD simulation using General Amber Force Field (GAFF) has been widely used.[52] The trajectories were evaluated along 200 ns simulation for the root-mean-square displacement (RMSD), atom contacts, hydrogen bonds (H-bonds), and radius of gyration (RoG) to see the quality of the system formed. The system stability was analyzed by plotting all atoms-RMSD fluctuations during the simulation.[53] The RMSD analysis was calculated on all atoms, backbone, and ligands (Fig. 6). The increasing fluctuation of all atoms-RMSD in each system showed as follows: 1NS-SIRT1 (range: 0-25 ns and 175-180 ns), DS1-SIRT1 (0-25 ns), and DS2-SIRT1 (0-15 ns). These changes indicated a conformational change in the complex structure during the simulation time. However, there was no significant change in the ligand coordinates at the SIRT1 binding site, as seen from the ligand-RMSD, which did not show any fluctuating changes. Overall, the last 40 trajectories (160-200 ns) showed good system stability, maintaining at ~0.3-0.4 nm, with a similar trend observed on all atoms-RMSD of the apoprotein (Fig. S2). Then, phase equilibrium was also measured by calculating the value of atom contacts and hydrogen bonds (Fig. 7). In detail, the average values for each system were 1NS-SIRT1 (atom contacts: 6 ± 2 and H-bonds: 4 ± 1), DS1-SIRT1 (atom contacts: 4 ± 3 and H-bonds: 3 ± 1), and DS2-SIRT1 (atom contacts: 4 ± 1 and H-bonds: 3 ± 2). Meanwhile, the RoG value

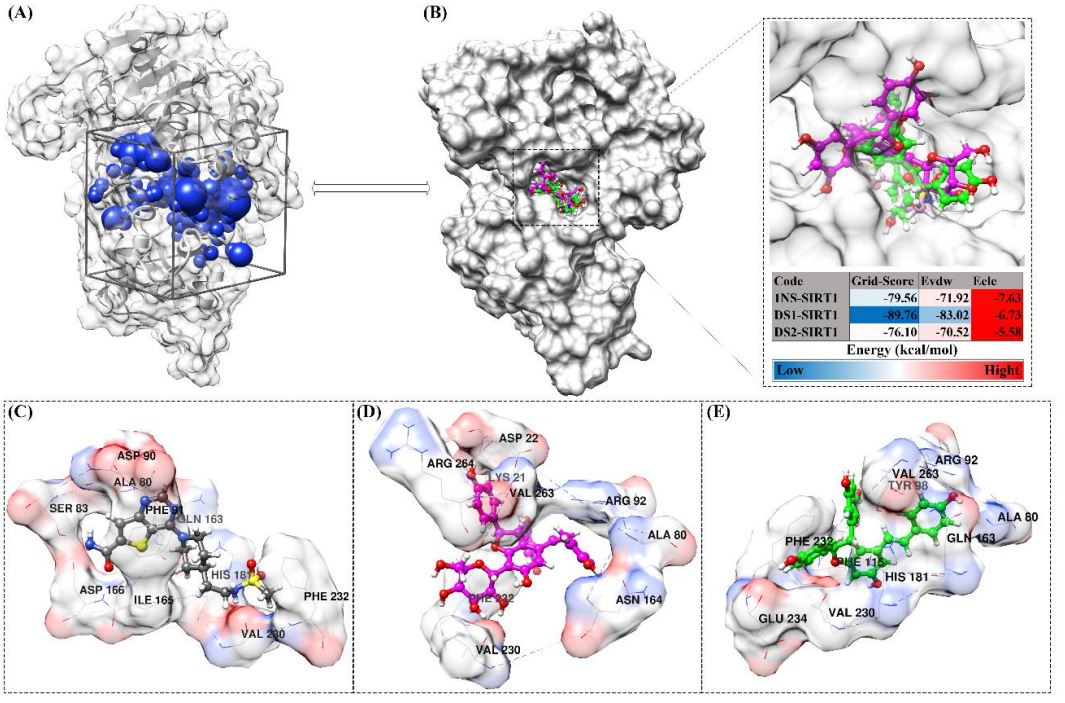

Fig. 5 Molecular docking analysis. (A) Grid-box preparation based on the coordinates of selected spheres, (B) Inhibitor –SIRT1 docking based on functional grid score, (C) The 1NS conformation on the SIRT1 binding site, (D) The DS1 conformation on the SIRT1 binding site, and (E) The DS2 conformation on the SIRT1 binding site.

showed fluctuation of each system by maintaining at ~2.1-2.2 nm (Figs. 7 and S2), indicating each system's rigidity and folding stability.

3.6 Free energy calculation

The binding affinity of inhibitors-SIRT1 was calculated using QM/MM-GBSA approach with DFTB as the theoretical level at 100 frames of the last 40 ns trajectories, and the results are listed in Table 4. These data implied the participation of ΔE_{vdW} and ΔG_{SCF} as the main contributors to the ΔG_{bind} complex, in which ΔE_{vdW} showed a stronger binding affinity of inhibitor-SIRT1 than ΔE_{elec}. Meanwhile, the solvation effect and entropy term showed a contribution to ΔG_{bind}, such as 1NS-SIRT1 (-21.44 kcal/mol), DS2-SIRT1 (-25.94 kcal/mol), and

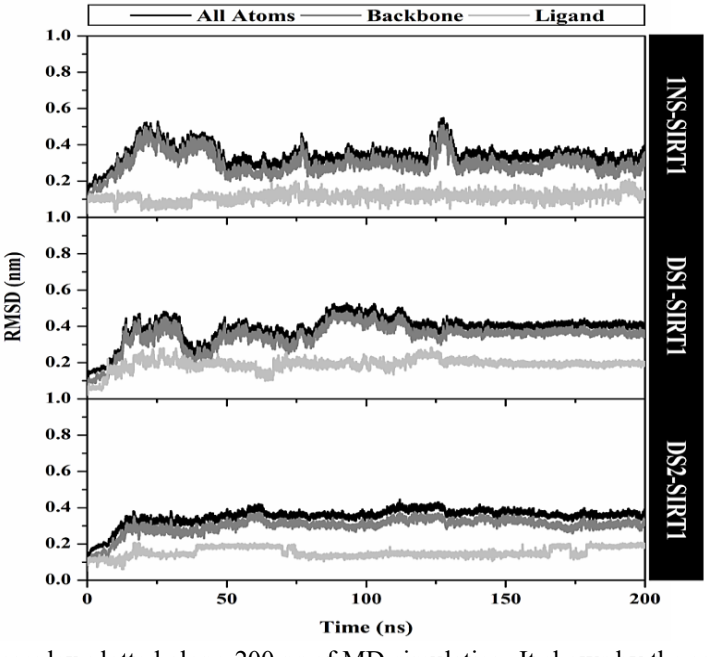

Fig. 6 System stability of each complex plotted along 200 ns of MD simulation. It shows by the root-mean-square displacement of all atoms, backbone (Cα, C, N, and O), and ligand.

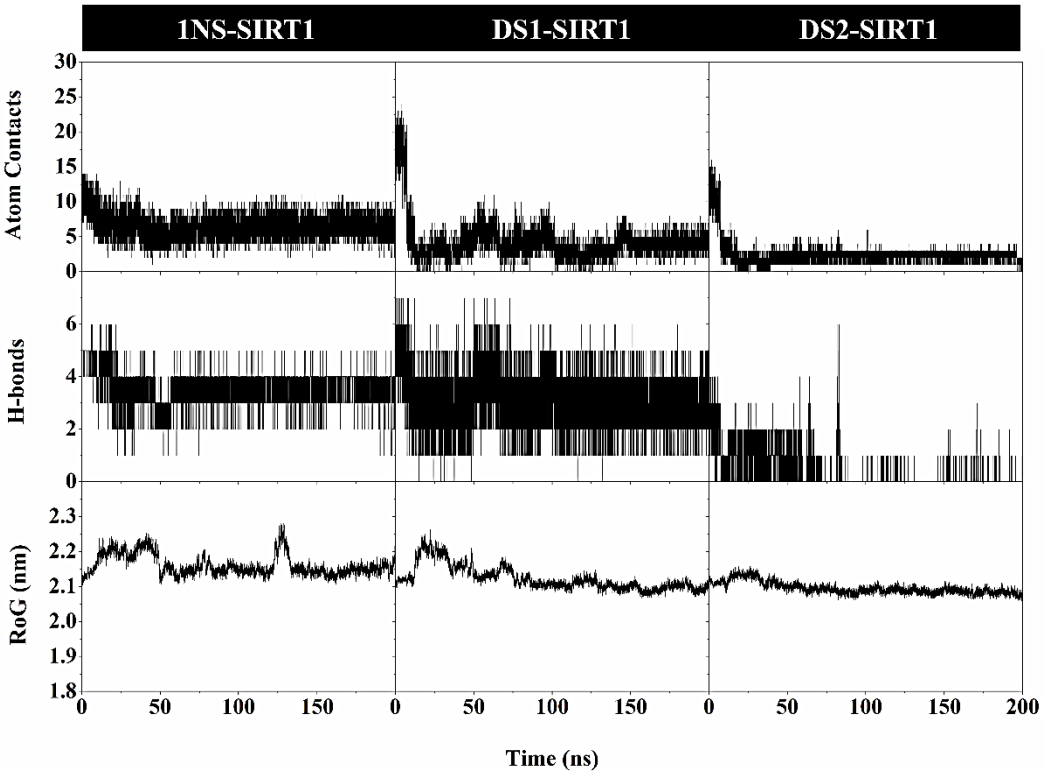

Fig. 7 Atom contacts, hydrogen bonds (H-bonds), and radius of gyration (RoG) were plotted along with a 200 ns MD simulation. Noted, atom contacts were calculated using a radius of 3.5 Å from the inhibitor coordinate. Meanwhile, the cut value of H-bonds was calculated using 3.5 Å and angle 120°.

affinity than DS1 on the SIRT1 as the focused target. In addition, the value of ΔG_{bind} DS1 was stronger than 1NS (-DS2-SIRT1 (-12.48 kcal/mol). The prediction results suggested the possibility of DS1 having a two-fold binding 21.44 kcal/mol) as a control with a difference of ΔG_{bind}: ~-4.50 kcal/mol. We found that the grid scores and ΔG_{bind} showed the same trend for each system, namely DS1-SIRT1 < 1NS-SIRT1 < DS2-SIRT1 (Fig. 5B and Table 4). In particular, DS1 showed a low binding affinity to the SIRT1 enzyme from a thermodynamic aspect. It was consistent with the results of a previously reported study, which showed that ε-viniferin did not have an inhibitory effect on the SIRT1 enzyme.[19] Conversely, a glucose group on the C-12b atom may be essential in increasing its binding affinity. Candidates with stronger ΔG_{bind} (more negative) can bind strongly to the active site of the targeted protein[54] and inhibit SIRT1 enzyme regulation, which has implications for cancer cell development.[11–16]

For the following evaluation process, the key residues involved in the inhibition process can be studied through per-residue decomposition energy ($\Delta G_{bind}^{residue}$).[41] The calculation for $\Delta G_{bind}^{residue}$ was carried out using the MM-GBSA approach based on the selected criteria. This study was performed on amino acid residues with a stable energy contribution, namely $\Delta G_{bind}^{residue}$ < -1.00 kcal/mol. The results revealed that several amino acids met the criteria and were partly responsible for the interaction with the inhibitor (Fig. 8). In detail, 1NS-SIRT1 (seven residues: Phe91, Phe115, Gln163, Asn164, Ile165, Asp166, and Val263), DS1-SIRT1 (eighteen residues: Ile12, Phe91, Arg92, Ile97, Pro111, Gln112, Met114, Phe115, Asn164, Ile165, Hie181, Ile229, Val230, Phe231, Phe232, Lys262, Val263, and Arg264), and DS2-SIRT1 (eleven residues: Lys21, Phe91, Arg92, Gln112, Phe115, Ile165, Hie181, Val230, Phe232, Val263, and Arg264). These results identified that DS1 interacted more with amino acid residues on the active site of SIRT1 than DS2. Perhaps this was mediated by the interaction of the glucose groups with more amino acid residues, such as Val230 and Phe232. Meanwhile, although 1NS showed the slightest interaction with amino acid residues, it had the most substantial $\Delta G_{bind}^{residue}$ value compared to DS2. It was demonstrated by amino acid residues Phe91 (-4.14 kcal/mol) and Ile165 (-4.05 kcal/mol). Overall, the energy contribution ($E_{vdW} + E_{ele}$) of each key residue is shown in Fig. 9. Consistent with the results of ΔG_{bind}, we found that the main contribution of the stabilization inhibitor was E_{vdW} ($\Delta E_{vdW} + \Delta G_{solv}^{nonpolar}$). It can be seen in E_{vdW} contribution reaching ~-4.13 kcal/mol as seen by the negative value despite the E_{ele} ($\Delta E_{ele} + \Delta G_{solv}^{ele}$) contribution looking relatively low. This information provided an essential parameter in

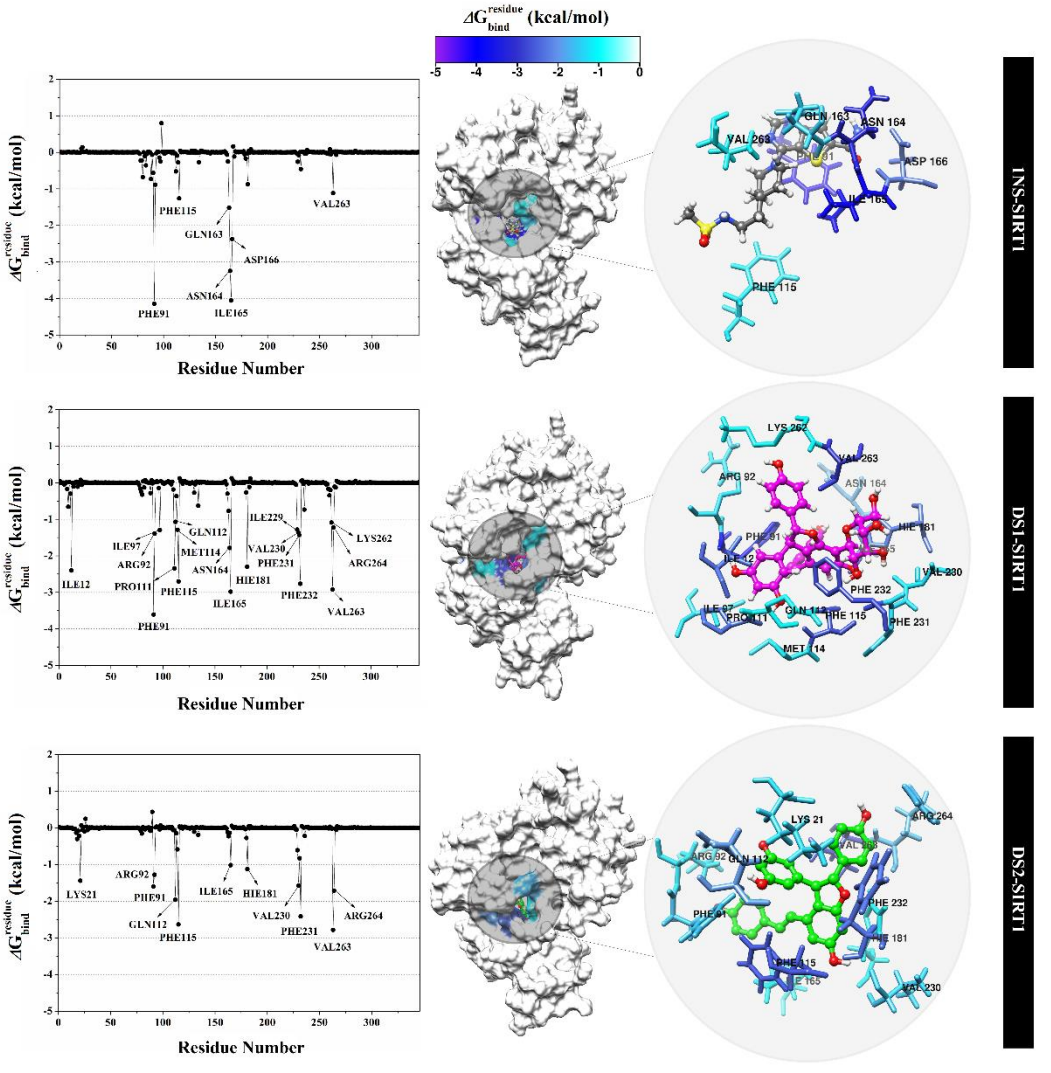

Fig. 8 Per-residue energy decomposition ($\Delta G_{bind}^{residue}$) was calculated using the MM-GBSA approach. The involved key residues are colored according to their $\Delta G_{bind}^{residue}$ values to stabilize interaction with the SIRT1 enzyme. The highest to lowest energy is represented by white to blue.

understanding the participation of key residues in the inhibitor stabilization in binding to the SIRT1 enzyme at the molecular level.

3.7 Interaction of the binding site: Water accessibility and hydrogen bond occupation

The water molecule's access to the active site of the targeted enzyme for Apo protein (SIRT1) and complex (inhibitor-SIRT1) was calculated through the solvent-accessible surface area (SASA). The SASA was calculated using the last 40 ns trajectories and the obtained result is depicted in Fig. 10. In detail, the average values indicated the SASA values of each system were SIRT1 (7.13 ± 0.62 nm^2), 1NS-SIRT1 (8.63 ± 0.69 nm^2), DS1-SIRT1 (9.50 ± 0.91 nm^2), and DS2-SIRT1 (11.77 ± 0.98 nm^2). Based on the average value of SASA, the presence of inhibitors on the active site of the SIRT1 enzyme indicated an increase in the number of water molecules on the SIRT1 active site. It illustrated that the displacement inhibitor on the SIRT1 active site was more likely to be accessed by water molecules than the one without an inhibitor (Apo protein). It needs to be noted that water molecule activity is significant in maintaining protein structure.[55]

Furthermore, hydrogen bonds (H-bonds) were calculated at the last 40 ns trajectories, and the obtained results are listed in Table 5. It should be noted that the presence of hydrogen bonds is essential in inhibitor-protein intramolecular interactions.[56–58] Based on the evaluation, a bond is considered a hydrogen bond if it has an occupancy percentage ≥ 25%, while the H-bond with decisive criteria is indicated by a percentage occupancy ≥ 75%.[59] The 1NS showed four H-bonds in the strong category; meanwhile, the DS1 showed two H-bonds, with one belonging to the solid H-bond category. The presence of a glucose group on the DS1 structure was necessary for the hydrogen bond interaction on the Val230

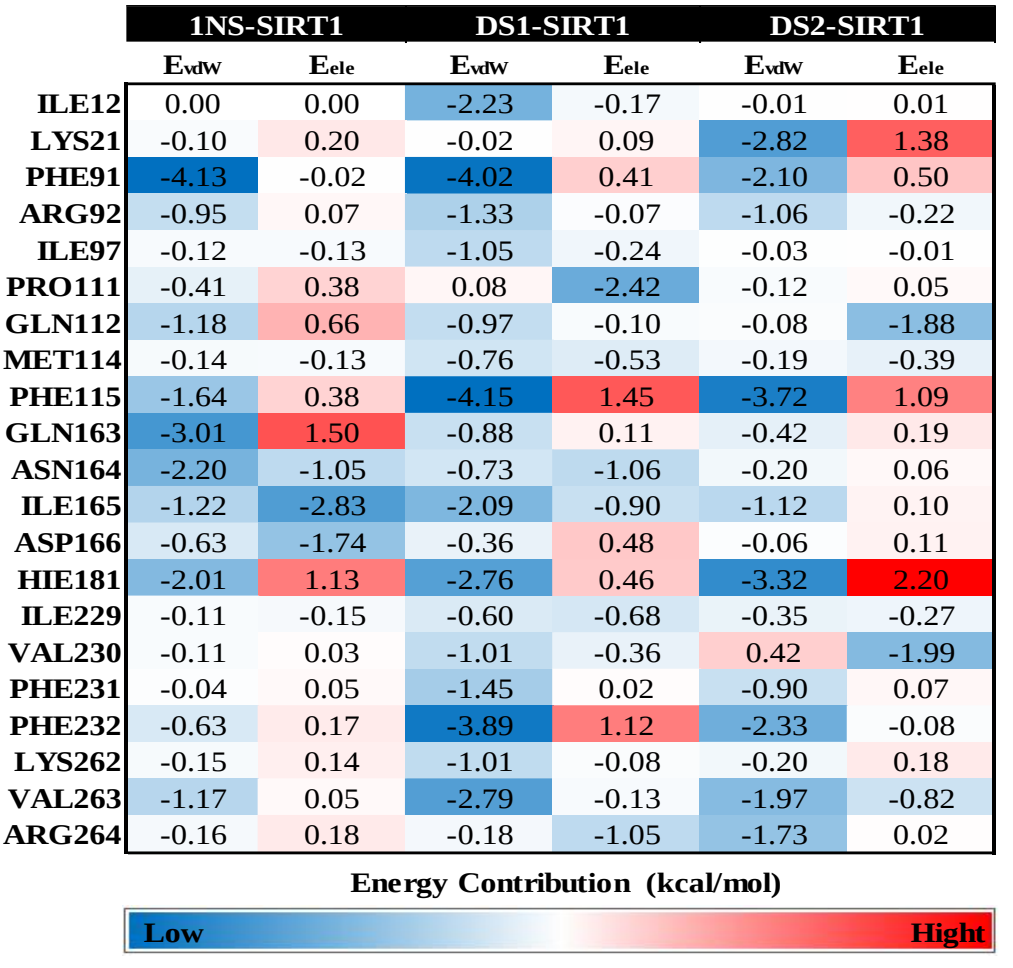

Fig. 9 Energy contribution was calculated using the MM-GBSA method. The van der Waals ($\Delta E_{vdW} + \Delta G_{solv}^{nonpolar}$) and electrostatic ($\Delta E_{ele} + \Delta G_{solv}^{ele}$) contribution energies were obtained from each key residue involved in the inhibitor-SIRT1 interaction on the binding site.

Table 4. Determination of energy component (kcal/mol) of each complex using the QM/MM-GBSA approach. Data are shown as mean ± standard error of the mean (SEM).

Energy component	1NS-SIRT1	DS1-SIRT1	DS2-SIRT1
QM/MM (DFTB)			
ΔE_{vdW}	-50.18 ± 0.30	-75.87 ± 0.32	-50.04 ± 0.34
ΔE_{ele}	0.24 ± 0.00	-0.07 ± 0.00	-0.31 ± 0.00
ΔG_{gas}	-49.93 ± 0.30	-75.95 ± 0.32	-50.36 ± 0.34
ΔG_{SCF}	-30.80 ± 0.54	-48.78 ± 0.39	-50.92 ± 0.43
GBSA			
ΔG_{solv}^{ele}	36.85 ± 0.50	74.05 ± 0.29	69.76 ± 0.28
$\Delta G_{solv}^{nonpolar}$	-5.49 ± 0.02	-10.09 ± 0.01	-7.07 ± 0.01
ΔG_{sol}	31.36 ± 0.49	63.96 ± 0.29	62.68 ± 0.27
NMODE			
$-T\Delta S$	27.94 ± 1.73	34.83 ± 0.90	26.11 ± 1.61
Free Energy			
ΔH	-49.38 ± 0.30	-60.77 ± 0.34	-38.59 ± 0.25
ΔG_{bind}	-21.44	-25.94	-12.48

Table 5. Hydrogen bonds analysis using 4000 frames from the last 40 ns trajectories. The cut value: distance 3.5 Å and angle 120°.

H-Bond Interaction	PO (%)	AD (Å)	AA (°)
1NS-SIRT1			
O17…H-N(ILE165)	99.92	2.82	163.24
(ASP166)OD2…H162-N16	98.02	2.94	158.25
N19…H-N(PHE91)	97.90	3.07	155.07
O17…G-N(ASP166)	94.60	3.10	148.12
DS1-SIRT1			
(VAL230)O…3'-OH	89.22	2.81	147.10
(VAL230)O…13b-OH	29.02	3.24	135.27
(VAL230)O…2'-OH	12.70	2.82	145.68
(ASN164)OD1…4b-OH	0.07	3.18	135.77
DS2-SIRT1			
4b-OH…HE-NE(ARG92)	0.77	3.25	131.50
4b-OH…H-N(ARG92)	0.55	3.19	143.19
(ARG92)NE…4b-OH	0.05	3.48	123.82

PO: Percentage occupancy, AD: Average distance, and AA: Average angle

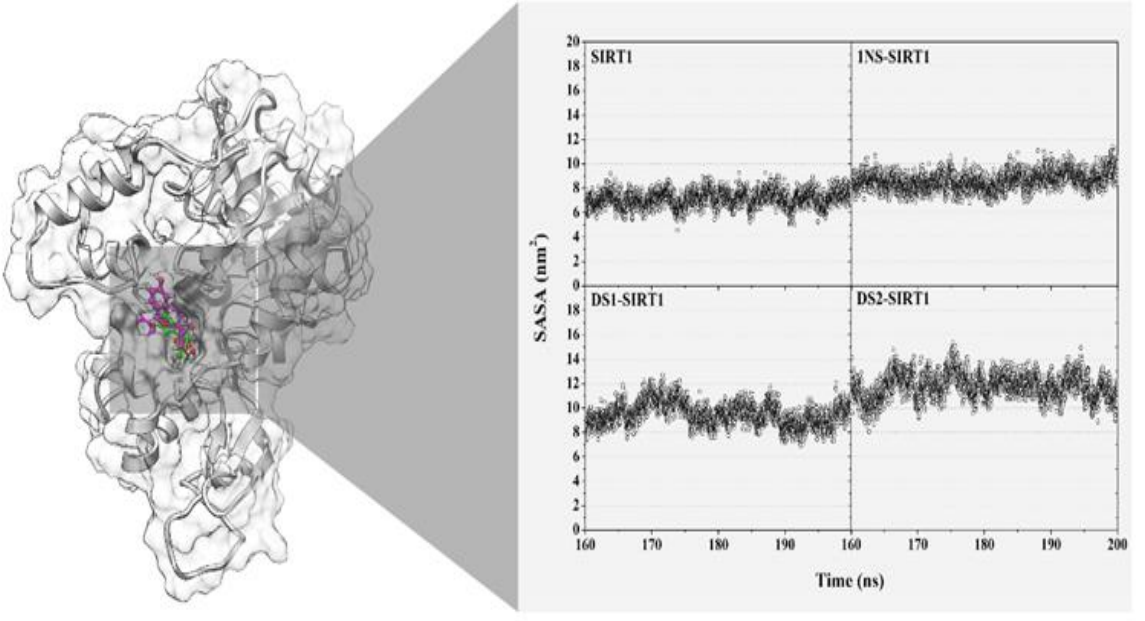

Fig. 10 The solvent-accessible surface area (SASA) using the last 40 ns trajectories. The surface of residues within 5 Å from each inhibitor was used to calculate the SASA in the SIRT1 active site.

residue. Compared to DS2, DS1 has an H-bond interaction that was not worth considering. This result was in line with the analyses of the Fukui function (Table S3) and MEP (Fig. 4), which indicated that 3'-OH and 13b-OH have a high chance of experiencing interaction. Therefore, a glucose group on C-12b of ε-viniferin enhanced the intermolecular interaction of the SIRT1 inhibitor.

4. Conclusions

Here we describe the differences between DS1 and DS2 in the forms of electronic structure properties and their interactions with the SIRT1 enzyme. Proton chemical shift was modeled using the B3LYP/6-311++G(d,p) approach and agreed with the experimental results. The presence of a glucose group in the DS1 structure increased the reactivity properties through Fukui function, MEP, and global reactivity analyses. Prediction of binding affinity and key residues of inhibitors against the SIRT1 enzyme was studied through molecular docking and MD simulation. The binding affinity prediction displayed a similar trend between the grid score and ΔG_{bind}, namely DS1-SIRT1 < 1NS-SIRT1 < DS2-SIRT1. Meanwhile, the calculation of $\Delta G_{bind}^{residue}$ showed 21 key residues (Ile12, Lys21, Phe91, Arg92, Ile97, Pro111, Gln112, Met114, Phe115, Gln163, Asn164, Ile165, Asp166, Hie181, Ile229, Val230, Phe231, Phe232, Lys262, Val263, and Arg264), which were responsible for stabilizing the interaction at the binding site of the SIRT1 enzyme. Furthermore, atomic interactions showed that the presence of a glucose group (3'-OH) could increase the interaction of the Val230 residue with a strong H-bond category (PO: 89.22%). In conclusion, a glucose group on the C-12b atom of ε-viniferin increased the inhibitory efficiency of SIRT1 compared to ε-viniferin.

Acknowledgments

We are grateful for this work's computational resources supported by UCoE Research Center for Bio-Molecule Engineering, Universitas Airlangga (BIOME-UNAIR). This study was supported by the research grant Program of "HIBAH RISET MANDAT 2022" from Universitas Airlangga. Contract Number: 214/UN3.15/PT/2022.

Conflict of Interest

There is no conflict of interest.

Supporting Information

Applicable.

References

[1] M. C. Haigis, D. A. Sinclair, Mammalian Sirtuins: Biological Insights and Disease Relevance, *Annual Review of Pathology: Mechanisms of Disease*, 2010, **5**, 253-295, doi: 10.1146/annurev.pathol.4.110807.092250

[2] V. Carafa, L. Altucci, A. Nebbioso, Dual tumor suppressor and tumor promoter action of sirtuins in determining malignant phenotype, *Frontiers in Pharmacology*, 2019, **9**, 1-14, doi: 10.3389/fphar.2019.00038.

[3] M. Roth, W. Y. Chen, Sorting out functions of sirtuins in cancer, *Oncogene*, 2014, **33**, 1609-1620, doi: 10.1038/onc.2013.120.

[4] L. Ruan, L. Wang, X. Wang, M. He, X. Yao, SIRT1 contributes to neuroendocrine differentiation of prostate cancer, *Oncotarget*, 2018, **9**, 2002-2016, doi: 10.18632/oncotarget.23111.

[5] L. F. Costa-Machado, P. J. Fernandez-Marcos, The sirtuin family in cancer, *Cell Cycle*, 2019, **18**, 2164-2196, doi: 10.1080/15384101.2019.1634953.

[6] N. Preyat, O. Leo, Sirtuin deacylases: a molecular link between metabolism and immunity, *Journal of Leukocyte Biology*, 2013, **93**, 669-680, doi: 10.1189/jlb.1112557.

[7] J. Yi, J. Luo, SIRT1 and p53, effect on cancer, senescence and beyond, *Biochimica et Biophysica Acta (BBA) - Proteins and Proteomics*, 2010, **1804**, 1684-1689, doi: 10.1016/j.bbapap.2010.05.002.

[8] J. Jeong, K. Juhn, H. Lee, S.-H. Kim, B.-H. Min, K.-M. Lee, M.-H. Cho, G.-H. Park, K.-H. Lee, SIRT1 promotes DNA repair activity and deacetylation of Ku70, *Experimental & Molecular Medicine*, 2007, **39**, 8-13, doi: 10.1038/emm.2007.2.

[9] E. Zhao, J. Hou, X. Ke, M. N. Abbas, S. Kausar, L. Zhang, H. Cui, The roles of sirtuin family proteins in cancer progression, *Cancers*, 2019, **11**, 1949, doi: 10.3390/cancers11121949.

[10] E. de Gregorio, A. Colell, A. Morales, M. Marí, Relevance of SIRT1-NF-κB axis as therapeutic target to ameliorate inflammation in liver disease, *International Journal of Molecular Sciences*, 2020, **21**, 3858, doi: 10.3390/ijms21113858.

[11] T. Liu, P. Y. Liu, G. M. Marshall, The critical role of the class III histone deacetylase SIRT1 in cancer, *Cancer Research*, 2009, **69**, 1702-1705, doi: 10.1158/0008-5472.CAN-08-3365.

[12] K. Rifaï, G. Judes, M. Idrissou, M. Daures, Y.-J. Bignon, F. Penault-Llorca, D. Bernard-Gallon, Dual SIRT1 expression patterns strongly suggests its bivalent role in human breast cancer, *Oncotarget*, 2017, **8**, 110922-110930, doi: 10.18632/oncotarget.23006.

[13] S. Liarte, J. L. Alonso-Romero, F. J. Nicolás, SIRT1 and estrogen signaling cooperation for breast cancer onset and progression, *Frontiers in Endocrinology*, 2018, **9**, 552, doi: 10.3389/fendo.2018.00552.

[14] X. Li, Z. Jiang, X. Li, X. Zhang, SIRT1 overexpression protects non-small cell lung cancer cells against osteopontin-induced epithelial-mesenchymal transition by suppressing NF-κB signaling, *OncoTargets and Therapy*, 2018, **11**, 1157-1171, doi: 10.2147/ott.s137146.

[15] D.-F. Yu, S.-J. Jiang, Z.-P. Pan, W.-D. Cheng, W.-J. Zhang, X.-K. Yao, Y.-C. Li, Y.-Z. Lun, Expression and clinical significance of Sirt1 in colorectal cancer, *Oncology Letters*, 2016, **11**, 1167-1172, doi: 10.3892/ol.2015.3982.

[16] F. Bi, N. Chen, J. Cao, W. Sun, Y. Zhou, C. Li, Q. Yang, A novel crosstalk between BRCA1 and sirtuin 1 in ovarian cancer, *Scientific Reports*, 2014, **4**, 1-7, doi: 10.1038/srep06666.

[17] J. S. Disch, G. Evindar, C. H. Chiu, C. A. Blum, H. Dai, L. Jin, E. Schuman, K. E. Lind, S. L. Belyanskaya, J. Deng, F. Coppo, L. Aquilani, T. L. Graybill, J. W. Cuozzo, S. Lavu, C. Mao, G. P. Vlasuk, R. B. Perni, Discovery of thieno[3, 2-d]pyrimidine-6-carboxamides as potent inhibitors of SIRT1, SIRT2, and SIRT3, *Journal of Medicinal Chemistry*, 2013, **56**, 3666-3679, doi: 10.1021/jm400204k.

[18] X. Zhao, D. Allison, B. Condon, F. Zhang, T. Gheyi, A. Zhang, S. Ashok, M. Russell, I. MacEwan, Y. Qian, J. A. Jamison, J. G. Luz, The 2.5 Å crystal structure of the SIRT1 catalytic domain bound to nicotinamide adenine dinucleotide (NAD+) and an indole (EX527 analogue) reveals a novel mechanism of histone deacetylase inhibition, *Journal of Medicinal Chemistry*, 2013, **56**, 963-969, doi: 10.1021/jm301431y.

[19] K. Hikita, N. Seto, Y. Takahashi, A. Nishigaki, Y. Suzuki, T. Murata, A. Loisruangsin, N. S. Aminah, Y. Takaya, M. Niwa, N. Kaneda, Effect of resveratrol dimers and tetramers isolated from vitaceous and dipterocarpaceous plants on human SIRT1 enzyme activity, *Natural Product Communications*, 2018, **13**, 1934578X1801301, doi: 10.1177/1934578x1801301130.

[20] A. Loisruangsin, K. Hikita, N. Seto, M. Niwa, Y. Takaya, N. Kaneda, Structural analysis of the inhibitory effects of polyphenols, (+)-hopeaphenol and (−)-isohopeaphenol, on human SIRT1, *BioFactors*, 2019, **45**, 253-258, doi: 10.1002/biof.1479.

[21] M. T. Borra, B. C. Smith, J. M. Denu, Mechanism of human SIRT1 activation by resveratrol, *Journal of Biological Chemistry*, 2005, **280**, 17187-17195, doi: 10.1074/jbc.m501250200.

[22] N. S. Aminah, S. A. Achmad, N. Aimi, E. L. Ghisalberti, E. H. Hakim, M. Kitajima, Y. M. Syah, H. Takayama, Diptoindonesin A, a new C-glucoside of ε-viniferin from shorea seminis (Dipterocarpaceae), *Fitoterapia*, 2002, **73**, 501-507, doi: 10.1016/s0367-326x(02)00179-x.

[23] M. I. Abdjan, N. S. Aminah, I. Siswanto, A. N. Kristanti, Y. Takaya, M. I. Choudhary, Exploration of stilbenoid trimers as potential inhibitors of sirtuin1 enzyme using a molecular docking and molecular dynamics simulation approach, *RSC Advances*, 2021, **11**, 19323-19332, doi: 10.1039/d1ra02233d.

[24] V. Salmaso, S. Moro, Bridging Molecular Docking to Molecular Dynamics in Exploring Ligand-Protein Recognition Process: An Overview, *Frontiers in Pharmacology*, 2018, **9**, 1-16, doi: 10.3389/fphar.2018.00923.

[25] C. Peng, J. Wang, Y. Yu, G. Wang, Z. Chen, Z. Xu, T. Cai, Q. Shao, J. Shi, W. Zhu, Improving the accuracy of predicting protein-ligand binding-free energy with semiempirical quantum chemistry charge, *Future Medicinal Chemistry*, 2019, **11**, 303-321, doi: 10.4155/fmc-2018-0207.

[26] J. Wang, Q. Shao, B. P. Cossins, J. Shi, K. Chen, J. Wang, Q. Shao, B. P. Cossins, J. Shi, K. Chen, Thermodynamics calculation of protein–ligand interactions by QM/MM polarizable charge

parameters, *Journal of Biomolecular Structure and Dynamics*, 2016, **1102**, 1-14, doi: 10.1080/07391102.2015.1019928.

[27] P.-C. Su, C.-C. Tsai, S. Mehboob, K. E. Hevener, M. E. Johnson, Comparison of radii sets, entropy, QM methods, and sampling on MM-PBSA, MM-GBSA, and QM/MM-GBSA ligand binding energies of F. tularensisenoyl-ACP reductase (FabI), *Journal of Computational Chemistry*, 2015, **36**, 1859-1873, doi: 10.1002/jcc.24011.

[28] A. J. Cohen, P. Mori-Sánchez, W. Yang, Challenges for density functional theory, *Chemical Reviews*, 2012, **112**, 289-320, doi: 10.1021/cr200107z.

[29] M. A. Izquierdo, J. Shi, S. Oh, S. Y. Park, B. Milian-Medina, J. Gierschner, D. Roca-sanjua, Excited-state non-radiative decay in stilbenoid compounds: an ab initio quantum-chemistry study on size and substituent effects, *Physical Chemistry Chemical Physics*, 2019, **21**, 22429-22439, doi: 10.1039/c9cp03308d.

[30] E. S. Kryachko, E. V. Ludeña, Density functional theory: foundations reviewed, *Physics Reports*, 2014, **544**, 123-239, doi: 10.1016/j.physrep.2014.06.002.

[31] D. E. V. Pires, T. L. Blundell, D. B. Ascher, pkCSM: predicting small-molecule pharmacokinetic and toxicity properties using graph-based signatures, *Journal of Medicinal Chemistry*, 2015, **58**, 4066-4072, doi: 10.1021/acs.jmedchem.5b00104.

[32] A. D. Becke, Density-functional thermochemistry. III. The role of exact exchange, *The Journal of Chemical Physics*, 1993, **98**, 5648-5652, doi: 10.1063/1.464913.

[33] K. Wolinski, J. F. Hinton, P. Pulay, Efficient implementation of the gauge-independent atomic orbital method for NMR chemical shift calculations, *Journal of the American Chemical Society*, 1990, **112**, 8251-8260, doi: 10.1021/ja00179a005.

[34] P. T. Thuy, N. T. Son, Thermodynamic study on antioxidative action of cynandione A: a DFT approach, *Structural Chemistry*, 2021, **32**, 1807-1817, doi: 10.1007/s11224-021-01756-4.

[35] D. Durga devi, S. Manivarman, S. Subashchandrabose, Synthesis, molecular characterization of pyrimidine derivative: a combined experimental and theoretical investigation, *Karbala International Journal of Modern Science*, 2017, **3**, 18-28, doi: 10.1016/j.kijoms.2017.01.001.

[36] W. J. Allen, T. E. Balius, S. Mukherjee, S. R. Brozell, D. T. Moustakas, P. T. Lang, D. A. Case, I. D. Kuntz, R. C. Rizzo, DOCK 6: impact of new features and current docking performance, *Journal of Computational Chemistry*, 2015, **36**, 1132-1156, doi: 10.1002/jcc.23905.

[37] S. R. Brozell, S. Mukherjee, T. E. Balius, D. R. Roe, D. A. Case, R. C. Rizzo, Evaluation of DOCK 6 as a pose generation and database enrichment tool, *Journal of Computer-Aided Molecular Design*, 2012, **26**, 749-773, doi: 10.1007/s10822-012-9565-y.

[38] J. A. Maier, C. Martinez, K. Kasavajhala, L. Wickstrom, K. E. Hauser, C. Simmerling, ff14SB: improving the accuracy of protein side chain and backbone parameters from ff99SB, *Journal of Chemical Theory and Computation*, 2015, **11**, 3696-3713, doi: 10.1021/acs.jctc.5b00255.

[39] T.-S. Lee, D. S. Cerutti, D. Mermelstein, C. Lin, S. LeGrand, T. J. Giese, A. Roitberg, D. A. Case, R. C. Walker, D. M. York, GPU-accelerated molecular dynamics and free energy methods in Amber18: performance enhancements and new features, *Journal of Chemical Information and Modeling*, 2018, **58**, 2043-2050, doi: 10.1021/acs.jcim.8b00462.

[40] D. R. Roe, T. E. Cheatham III, PTRAJ and CPPTRAJ: software for processing and analysis of molecular dynamics trajectory data, *Journal of Chemical Theory and Computation*, 2013, **9**, 3084-3095, doi: 10.1021/ct400341p.

[41] B. R. Miller III, T. D. McGee Jr, J. M. Swails, N. Homeyer, H. Gohlke, A. E. Roitberg, MMPBSA.py: an efficient program for end-state free energy calculations, *Journal of Chemical Theory and Computation*, 2012, **8**, 3314-3321, doi: 10.1021/ct300418h.

[42] E. Wang, H. Sun, J. Wang, Z. Wang, H. Liu, J. Z. H. Zhang, T. Hou, End-point binding free energy calculation with MM/PBSA and MM/GBSA: strategies and applications in drug design, *Chemical Reviews*, 2019, **119**, 9478-9508, doi: 10.1021/acs.chemrev.9b00055.

[43] Y. Han, J. Zhang, C. Q. Hu, X. Zhang, B. Ma, P. Zhang, In silico ADME and toxicity prediction of ceftazidime and its impurities, *Frontiers in Pharmacology*, 2019, **10**, 434, doi: 10.3389/fphar.2019.00434.

[44] T. Blood, B. Barrier, R. Daneman, A. Prat, The Blood–Brain Barrier, *Cold Spring Harbor Perspectives in Biology*, 2015, **7**, a020412, doi: 10.1101/cshperspect.a020412.

[45] M. G. Siskos, M. I. Choudhary, I. P. Gerothanassis, DFT-calculated structures based on 1H NMR chemical shifts in solution vs. structures solved by single-crystal X-ray and crystalline-sponge methods: assessing specific sources of discrepancies, *Tetrahedron*, 2018, **74**, 4728-4737, doi: 10.1016/j.tet.2018.07.038.

[46] T. Venianakis, C. Oikonomaki, M. G. Siskos, A. Primikyri, I. P. Gerothanassis, DFT calculations of 1H NMR chemical shifts of geometric isomers of conjugated linolenic acids, hexadecatrienyl pheromones, and model triene-containing compounds: structures in solution and revision of NMR assignments, *Molecules*, 2021, **26**, 3477, doi: 10.3390/molecules26113477.

[47] L. A. de Souza, W. M. G. Tavares, A. P. M. Lopes, M. M. Soeiro, W. B. de Almeida, Structural analysis of flavonoids in solution through DFT 1H NMR chemical shift calculations: Epigallocatechin, Kaempferol and Quercetin, *Chemical Physics*

Letters, 2017, **676**, 46-52, doi: 10.1016/j.cplett.2017.03.038.
[48] L. A. De Souza, H. C. Da Silva, W. B. De Almeida, Structural determination of antioxidant and anticancer flavonoid rutin in solution through DFT calculations of 1H NMR chemical shifts, *ChemistryOpen*, 2018, **7**, 902-913, doi: 10.1002/open.201800209.
[49] R. N. Guzzo, M. J. C. Rezende, V. Kartnaller, J. W. de M Carneiro, S. R. Stoyanov, L. M. da Costa, Experimental and DFT evaluation of the 1H and 13C NMR chemical shifts for calix[4]arenes, *Journal of Molecular Structure*, 2018, **1157**, 97-105, doi: 10.1016/j.molstruc.2017.12.038.
[50] J. Frau, F. Muñoz, D. Glossman-Mitnik, A molecular electron density theory study of the chemical reactivity of cis- and trans-resveratrol, *Molecules*, 2016, **21**, 1650, doi: 10.3390/molecules21121650.
[51] T. P. Thi, S. N. The, Antioxidant of Trans-Resveratrol: A Comparison between OH and CH Groups Based on Thermodynamic Views, *Journal of Chemistry*, 2020, **2020**, 1-15, 10.1155/2020/8869023.
[52] J. Wang, R. M. Wolf, J. W. Caldwell, P. A. Kollman, D. A. Case, Development and testing of a general amber force field, *Journal of Computational Chemistry*, 2004, **25**, 1157-1174, doi: 10.1002/jcc.20035.
[53] I. Aier, P. K. Varadwaj, U. Raj, Structural insights into conformational stability of both wild-type and mutant EZH2 receptor, *Scientific Reports*, 2016, **6**, 1-10, doi: 10.1038/srep34984.
[54] X. Du, Y. Li, Y. L. Xia, S. M. Ai, J. Liang, P. Sang, X. L. Ji, S. Q. Liu, Insights into Protein–Ligand Interactions: Mechanisms, Models, and Methods, *International Journal of Molecular Sciences*, 2016, **17**, 1-34, doi: 10.3390/ijms17020144.
[55] T. Vajda, A. Perczel, Role of water in protein folding, oligomerization, amyloidosis and miniprotein, *Journal of Peptide Science*, 2014, **20**, 747-759, doi: 10.1002/psc.2671.
[56] H. Chen, Y. Wang, Z. Gao, W. Yang, J. Gao, Assessing the performance of three resveratrol in binding with SIRT1 by molecular dynamics simulation and MM/GBSA methods: the weakest binding of resveratrol 3 to SIRT1 triggers a possibility of dissociation from its binding site, *Journal of Computer-Aided Molecular Design*, 2019, **33**, 437-446, doi: 10.1007/s10822-019-00193-0.
[57] B. Nutho, S. Pengthaisong, A. Tankrathok, V. S. Lee, J. R. Ketudat Cairns, T. Rungrotmongkol, S. Hannongbua, Structural basis of specific glucoimidazole and mannoimidazole binding by Os3BGlu7, *Biomolecules*, 2020, **10**, 907, doi: 10.3390/biom10060907.
[58] A. Azminah, L. Erlina, M. Radji, A. Mun, R. Riadhi, In silico and in vitro identification of candidate SIRT1 activators from Indonesian medicinal plants compounds database, *Computational Biology and Chemistry*, 2019, **83**, 107096, 10.1016/j.compbiolchem.2019.107096.
[59] J. Kästner, H. H. Loeffler, S. K. Roberts, M. L. Martin-Fernandez, M. D. Winn, Ectodomain orientation, conformational plasticity and oligomerization of ErbB1 receptors investigated by molecular dynamics, *Journal of Structural Biology*, 2009, **167**, 117-128, doi: 10.1016/j.jsb.2009.04.007.

Author Information

Muhammad Ikhlas Abdjan *is a Ph.D. student since 2021 under the guidance of professor Dr. Nanik Siti Aminah in the Doctoral Program in Mathematics and Natural Sciences, Faculty of Science and Technology, Universitas Airlangga (Indonesia). The focus of his doctoral research is drug design based on computational studies.*

Nanik Siti Aminah *is a full professor at the Department of Chemistry, Faculty of Science and Technology Universitas Airlangga (Indonesia). Her field of interest covers: Natural Product Chemistry, Organic Chemistry, and Green Chemistry. She has published many articles in his domain in well-reputed publishers. Currently, her research group focuses on looking at the activity of compounds from natural products as potential drug candidates.*

Alfinda Novi Kristanti *is an associate professor at the Department of Chemistry, Faculty of Science and Technology Universitas Airlangga (Indonesia). Her current researches focus on Natural Product Chemistry, Organic Chemistry for drug development. Additionally, she is a senior researcher at Biotechnology of Tropical Medicinal Plan Research Group, Universitas Airlangga.*

Imam Siswanto *is a lecturer in the chemistry department, Faculty of Science and Technology Universitas, Airlangga (Indonesia). The research focus is computational chemistry, including QSAR, molecular docking, and molecular dynamics simulation for drug design purposes. Additionally, he is also a director of the Bioformatic laboratory, UCoE Research Center for Bio-Molecule Engineering (BIOME),*

Universitas Airlangga.

Mirza Ardella Saputra *is a young lecturer in the nanotechnology engineering department, Faculty of Advanced Technology and Multidiscipline, Universitas Airlangga (Indonesia). Her current researches focus on organic Chemistry (natural product isolation and organic synthesis).*

Yoshiaki Takaya *is an associate professor at the faculty at pharmacy, Meijo University (Japan). His field of interest covers: Phytochemistry and organic chemistry. He has published more than 170 articles in well-reputed publishers.*